Proceedings of the 9th World Congress on Momentum, Heat and Mass Transfer (MHMT'24)
London, United kingdom – April 11 – 13, 2024
Paper No. ENFHT 277
DOI: 10.11159/enfht24.277

Energy and Exergy Assessment of Nanofluids in Solar Energy Harvesting

Roy Issa
West Texas A&M University
Canyon, Texas, United States of America
rissa@wtamu.edu

Abstract - Nanofluids were prepared in a water-base fluid using different types of nanoparticles that included CuO, Ag, ZnO, and MtNs at different concentrations. With the use of a solar simulator, experimental studies were performed to evaluate the thermal and exergetic efficiencies of the nanofluids. The nanofluid samples were subjected to an average heat flux of 800 W/m^2. The photothermal conversion efficiency was shown to peak at relatively low concentrations for the different nanoparticles, and was shown to decrease with the increase in the nanofluid temperature. Whereas the exergetic efficiency was shown to increase with the increase in temperature, reaching a peak at a temperature close to 40 ^{o}C for all nanofluids, and declining afterwards. Compared to distilled water, the enhancement in the average exergetic efficiency of the tested nanofluids concentrations was shown to narrowly range between 57% and 69%, higher than that of the photothermal conversion efficiency that was seen to range between 28% and 66%. Compared to other nanoparticles, silver had the highest of the thermal and exergetic efficiency reaching an average enhancement of 66% in the photothermal conversion efficiency at a concentration of 0.31% by weight, and 68% in its exergetic efficiency at the same concentration.

***Keywords*:** Nanofluid, Photothermal, Efficiency, Solar Simulator

1. Introduction

The efficient harvesting of direct solar energy depends on the working fluid used in the thermal system, and is a key factor in maximizing the utilization of this energy. Nanofluids, formed by the dispersion of nanoparticles in a base fluid, are shown to alter the thermophysical properties of the base fluid by enhancing the bulk fluid heat transfer capability. In addition, certain nanofluids are shown to exhibit outstanding photothermal conversion performance in harvesting direct solar energy.

Photoexcitation is the driving force that triggers the photothermal energy conversion process causing the material to build-up heat as a result. Photothermal energy conversion can be classified into three types based on the light absorption range [1]: plasmonic localized heating, non-radiative relaxation in semiconductors, and thermal vibration in molecules. In plasmonic localized heating, an immediate increase in localized temperature is caused by irradiating metallic nanoparticles at their resonance wavelength causing the electron gas to oscillate rapidly. During irradiation of semiconducting materials, excited electrons release energy either as photons or phonons (heat), similar to the energy of the bandgap. When it comes to thermal vibration in molecules, solar energy is converted to lattice vibration by organic materials. Due to the absorption and scattering of photons by the nanoparticles, the presence of nanoparticles within a nanofluid reduces the transmittance of photons when it is irradiated [2]. As nanofluid concentration increases, transmittance decreases while optical absorption increases. There is much wider range of wavelengths of optical absorption in the nanofluid than in the base fluid [2]. As a result, nanofluids are much better at optical absorption and photothermal conversion than their base fluid counterparts.

Researchers have studied the photothermal conversion efficiency of a wide variety of mono-type nanoparticles. These included Al_2O_3 [3-5], Au [6-11], Ag [3, 4, 7, 12-14], TiN (titanium nitride) [15], MWCNT (multi-walled carbon nanotubes) [3, 16-17] , Fe [4], Fe_3O_4 [18], TiO_{2-x} (oxygen deficient titanium dioxide) [3, 19], Si [4], SiO_2 [3], Gr (graphene) [17], GrO (graphene oxide) [20-22], SLGr [21], Cu [3-4], CuO [23], and CuO-MS [23]. In the above reported studies, the enhancement in the photothermal conversion efficiency varied from 13 to 50% for Al_2O_3 nanofluids, 20 to 311% for Au nanofluids, 7.4 to 275% for Ag nanofluids, 41 to 63% for TiN, 51 to 67% for MWCNT, 70% for Fe, 40 to 67% for Fe_3O_4, 9 to 36% for TiO_{2-x}, 29% for Si, 49% for SiO_2, 360% for Gr, 7 to 172% for GrO, 189% for SLGr, 44 to 52% for Cu, 6 to 56% for CuO, and 14 to 82% for CuO-MS. The mono-type nanofluids based on Au, Ag, Gr, and Gro are shown to exhibit photothermal conversion efficiency enhancements that can exceed 100%. Based on those studies, gold nanoparticle volume concentrations in a water-based fluid varied from 10-5% to 0.018%, silver nanofluid volume concentrations varied from 10-4% to 0.3%, and Gr and

GrO nanofluid volume concentrations varied from 0.001% to 0.01%. It is shown in those studies that as volume concentration increases, the photothermal conversion efficiency of the majority of these nanofluids increases up to a certain point. Using Al_2O_3 nanofluids as an example, the photothermal efficiency enhancement is shown to saturate around 50% at 2% volume concentration [3], while with MWCNT nanofluids, it is shown to saturate around 76% at 1% volume concentration [16]. In contrast, silver nanofluids exhibit a decreasing photothermal efficiency with increasing nanoparticle concentrations. According to the literature review, the photothermal conversion efficiency increased to 275% at 0.01% volume concentration, but declined with increasing concentration until saturation was reached at 0.3% volume concentration. Whereas at just 0.018% volume concentration, gold nanofluids exhibit 300% increase in photothermal efficiency.

As shown above, there are abundance of studies conducted on solar collectors structures and working fluids, but very limited studies have been conducted on exergy and energy comparison under different concentration levels to determine where the quality of energy is lost. The purpose of this study is to experimentally investigate the performance of certain types of nanofluids for both their thermal and exergetic efficiencies in a solar collector system.

2. Experimental Setup

A solar simulator (Model TS-3000 by MarsHydro) of dimensions 64 cm x 58 cm utilizing 450 W Light-Emitting Diodes (LEDs) was selected for the study (Fig. 1). The simulator provides a coverage area of 1.2 m x 1.2 m while emitting most of the light in the 400 to 700 nm spectrum band (Fig. 2). In order to map the radiation heat flux intensity of the solar simulator, a board of dimensions 38 cm x 30.5 cm x 2.75 cm was divided into 1.7 cm x 1.7 cm grids for the heat flux data to be gathered at each grid point. Solar radiation intensity was measured using Solar Survey 200R Irradiance Meter by Seaward Electronic Ltd. Figure 3 shows the map of the solar simulator heat flux intensity at a distance of 7 cm from the solar simulator. At this distance, the heat flux intensity is shown to have an average of 801 W/m^2, a minimum of 706 W/m^2 and a maximum of 895 W/m^2.

Fig. 1: Solar simulator [24].

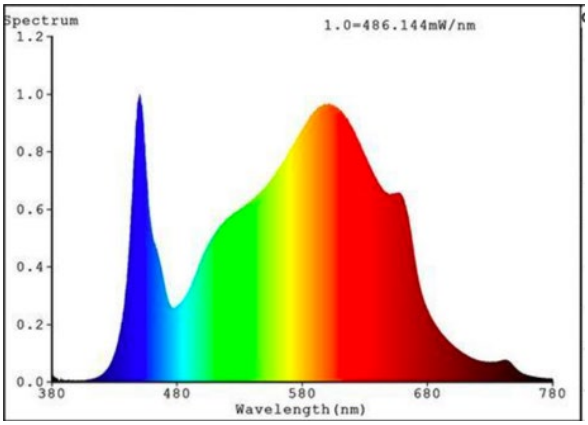

Fig. 2: Solar simulator light spectrum band [24].

Mapping data	2.75 in (From Panel to device)										Units	W/m^2			Temperature Range: 57 Celsius (80 min run)							
18	768	763	760	717	738	746	756	718	718	726	714	710	714	726	706	718	737	717	733	729	732	740
17	742	752	749	769	770	765	768	753	758	760	761	762	757	768	768	764	764	772	774	764	767	755
16	774	774	772	771	772	765	760	758	759	757	762	750	752	755	756	758	766	770	768	768	732	752
15	761	755	749	764	762	750	758	739	751	746	752	756	750	750	760	764	775	780	793	785	782	747
14	794	796	798	799	794	792	786	786	786	791	782	781	781	779	795	800	800	791	731	809	822	806
13	807	817	827	824	828	833	822	823	828	831	838	835	835	822	836	836	847	861	862	862	853	840
12	845	844	850	854	850	840	840	837	836	843	851	852	844	839	849	844	873	882	885	895	894	877
11	802	818	825	827	829	832	842	831	834	819	822	829	831	831	831	843	852	860	869	879	868	855
10	801	805	815	826	837	832	832	835	823	814	809	803	810	808	818	828	838	849	849	855	843	801
9	774	785	788	801	804	806	806	812	809	814	816	814	811	811	811	812	823	826	829	839	840	828
8	788	790	798	812	812	818	815	817	806	808	816	810	811	817	812	817	817	830	829	823	815	799
7	805	816	820	825	823	822	828	822	818	818	816	815	810	809	818	820	823	830	821	808	794	776
6	827	821	816	823	811	817	814	818	817	815	818	815	809	808	812	825	829	824	829	825	815	820
5	822	823	819	813	807	816	811	809	810	815	815	815	806	809	810	823	837	825	823	821	816	805
4	831	830	823	825	815	823	813	811	808	815	803	814	810	810	820	830	831	830	832	828	818	812
3	808	816	809	809	805	803	803	794	797	802	804	802	804	805	805	820	829	837	826	827	815	803
2	793	793	795	797	793	786	784	777	780	789	788	785	785	794	797	804	802	810	809	802	790	781
1	757	761	759	762	759	760	756	748	756	762	761	756	757	765	774	774	782	790	780	767	766	760
0	1	2	3	4	5	6	7	8	9	10	11	12	13	14	15	16	17	18	19	20	21	22

Fig. 3: Map of the solar simulator heat flux intensity in W/m^2 at 2.75" distance.

Figure 4 shows the design of the solar collector. The collector consists of 8 PVC tubes forming 8 passes with the fluid entering and exiting from the same side. Each tube has a length of 23.5 cm, an internal diameter of 1.5 cm and an external diameter of 1.7 cm. The experimental setup is shown in Fig. 5, and the details of the closed-loop system is shown in Fig. 6. A reflective tent was used to increase the irradiance heat flux on the targeted collector. The solar collector is positioned 7 cm under the solar simulator. It is then connected to a closed loop system using an external reservoir and a circulating pump. The total volume of the circulating fluid used in the system is 0.0012 m^3 (1.2 litres) and the mass flow rate is 0.062 kg/s. Six K-type thermocouples were positioned at the following locations to record the transient temperature: at the entry and exit sides of the solar collector, at the mid-section of tubes number 3 and 6, in the reservoir and in the ambient air.

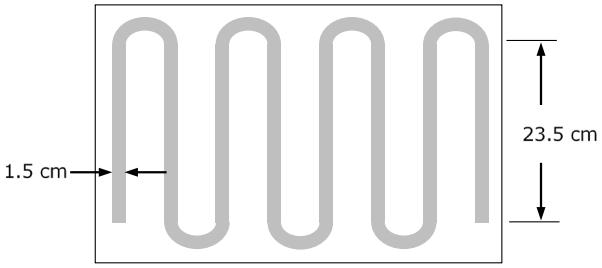

Fig. 4: Solar collector.

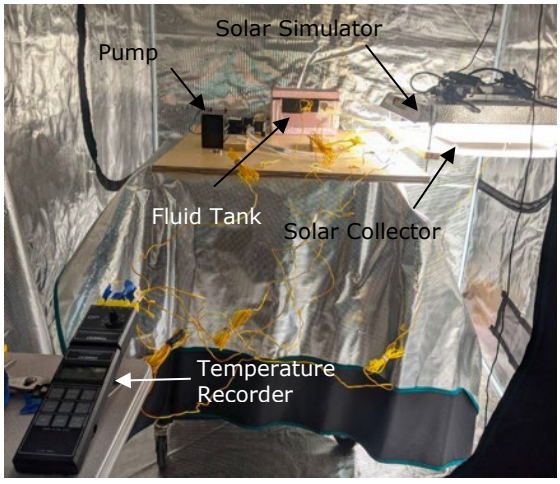

Fig. 5: System experimental setup.

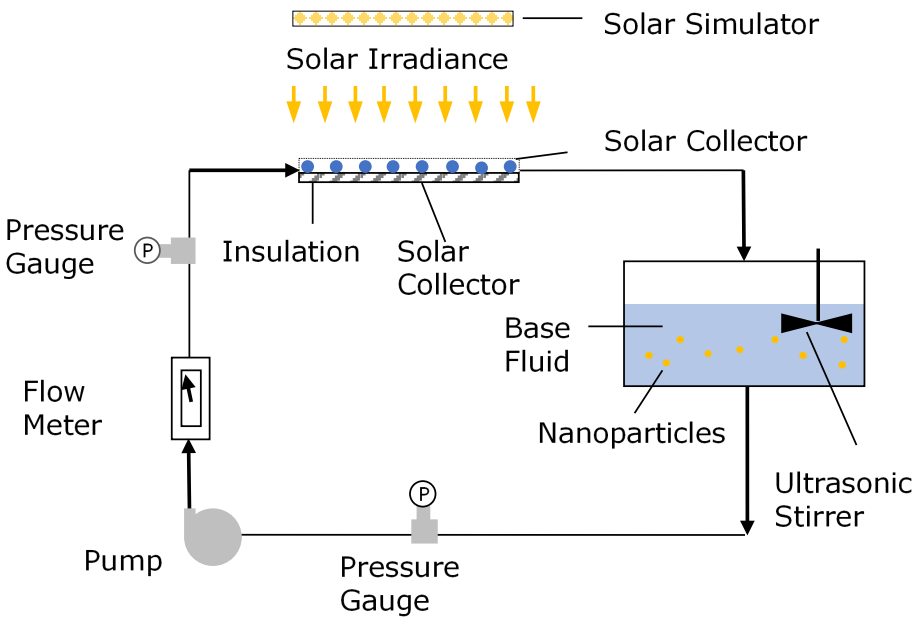

Fig. 6: Closed-loop system.

Several types of nanoparticles were tested for their photothermal conversion efficiency. These included Ag, CuO, ZnO, and MtNs nanoparticles. The concentration and size of these nanoparticles are shown in Table 1. After the nanoparticles were weighted in a beaker, they were mixed with few droplets of deionized water to create a paste. A rod was used to break the aggregates in the paste into small fragments that are then diluted with deionized water to the specified concentration. The test sample were then be ultra-sonicated for an hour to create a thoroughly dispersed nanofluid.

Table 1: Tested nanoparticles.

Nanoparticle	Description	Concentration (% wt)	Size
MtNS	Montmorillonite Nanosheets	0.25, 0.5	< 25 mm
ZnO	Zinc Oxide	0.1, 0.2	10 – 30 nm
CuO	Copper Oxide	3.1	40 nm
Ag	Silver Nanoparticles	0.1, 0.21, 0.31, 0.42	20-30 nm

3. Thermal and Exergetic Efficiencies

The particles were tested for their photothermal conversion efficiency. The photothermal conversion efficiency, η, is calculated as:

$$\eta = \frac{(c_b m_b + c_n m_n)\Delta T}{GA\Delta t} \tag{1}$$

where c_b and c_n are the specific heat of the base fluid and nanoparticles respectively, m_b and m_n are the masses of the base fluid and nanoparticles respectively, ΔT is the temperature rise of the bulk fluid in a time interval of Δt. A is the illumination area of the fluid and G is the incident solar flux. The specific heat of the nanofluid was calculated using the thermal equilibrium model proposed by Xuan and Roetzel [25]:

$$c_n = \frac{\rho_b c_b (1-\phi) + \rho_n c_n \phi}{\rho_n} \tag{2}$$

where,

$$\rho_n = \rho_b(1-\phi) + \rho_n\phi \tag{3}$$

The exergetic efficiency of the solar collector, η_{ex}, is determined from the ratio of useful exergy output, $E_{x,u}$, to input exergy supplied by the solar simulator, $E_{x,sol}$:

$$\eta_{ex} = \frac{E_{x,u}}{E_{x,in}} = 1 - \frac{E_{x,dest}}{E_{x,sol}} \tag{4}$$

where $E_{x,sol}$ is the exergy associated with the heat input from the solar simulator:

$$E_{x,sol} = \left(1 - \frac{T_a}{T_{sol}}\right)\dot{Q}_{sol} \tag{5}$$

T_a is the ambient temperature, T_{sol} is the solar simulator surface temperature, and $\dot{Q}_{sol}$ is the solar power absorbed by the collector. Exergy due to destruction is calculated as follows:

$$E_{x,dest} = T_a\dot{s}_{gen} \tag{6}$$

where,

$$\dot{s}_{gen} = \dot{m}c_p ln\frac{T_o}{T_i} - \frac{\dot{Q}_{sol}}{T_{sol}} + \frac{\dot{Q}_o}{T_a} \tag{7}$$

where $\dot{Q}_o$ is the heat loss to the surrounding air given by:

$$\dot{Q}_o = \dot{Q}_{sol} - \dot{m}c_p(T_o - T_i) \tag{8}$$

4. Experimental Tests

Heat transfer tests were performed on the different nanofluid samples that were prepared. In each test, the nanofluid was circulated in the closed-loop system at a mass flow rate of 0.062 kg/s while the solar collector was subjected to incident radiation from the solar simulator for 75 minutes. For all tests, the nanofluid samples were subjected to an average heat flux of approximately 800 W/m^2. Temperature was also recorded at the various locations mentioned earlier. Figure 7 shows the temperature gain of the different nanofluids along with the case of distilled water. Compared to distilled water, nanofluids show substantial increase in temperature gain. Figure 8 shows the photothermal conversion efficiency as function of the nanofluid average temperature. Among the best performing fluids is the nanofluid sample with 0.31% by weight Ag nanoparticles, followed by the nanofluid sample with 0.1% by weight ZnO nanoparticles, and followed by the sample with 3.1% by weight CuO nanoparticles. Figure 8 shows the photothermal conversion efficiency to decrease with the increase in the fluid temperature.

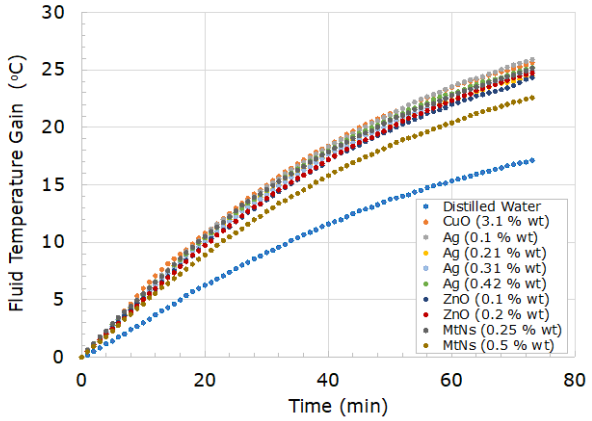

Fig. 7: Nanofluid temperature gain versus time.

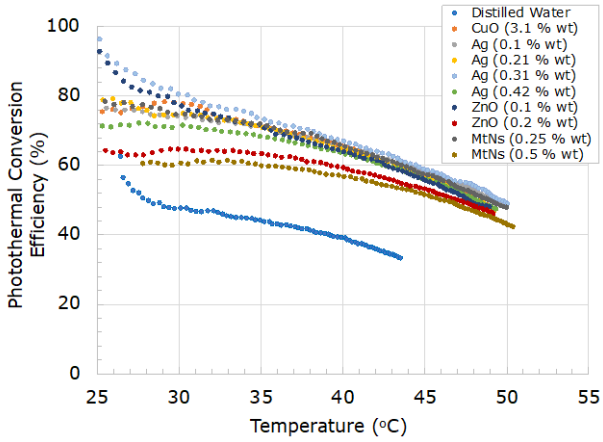

Fig. 8: Nanofluid photothermal conversion efficiency versus temperature.

Figure 9 shows a comparison in the photoconversion efficiency between the different samples. In the limited tests that were performed, silver with concentration of 0.31% by weight performed the best among the different silver concentrations that were tested (0.1 to 0.42 %wt), while ZnO and MtNs at their lowest concentrations (0.1 %wt and 0.25 %wt, respectively) performed the best. CuO nanofluid was tested at a concentration of only 3.1 %wt. At this concentration, its photothermal convergence performance was relatively close to the best performance of the ZnO and MtNs nanofluid samples. Figure 10 shows the exergetic efficiency of the nanofluid samples as function of the fluid average temperature. For all samples, the exergetic efficiency is shown to reach a peak at a temperature close to 40 °C and decline with further increase in temperature. The efficiency is shown to range between 2% and 13% as the fluid temperature ranges between 23 °C and 50 °C.

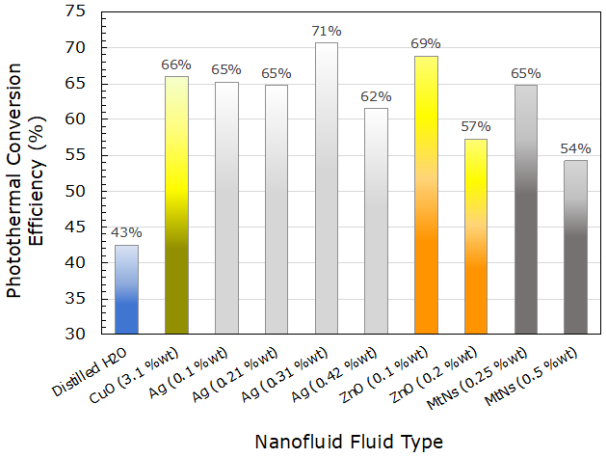

Fig. 9: Average photothermal conversion efficiency of different nanofluids fluids.

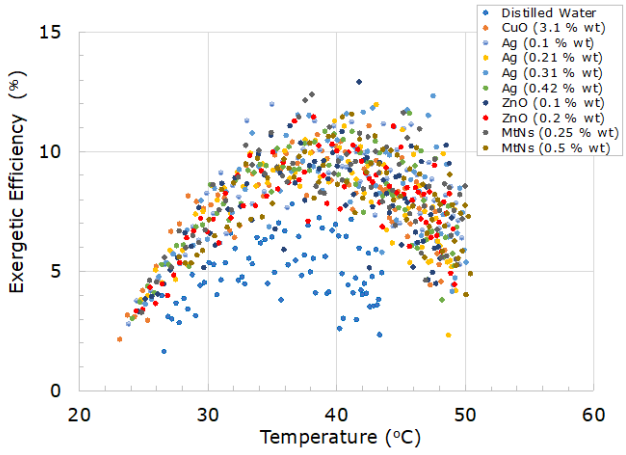

Fig. 10: Nanofluid exergetic efficiency versus temperature.

Figures 11 and 12 show the enhancement in the photothermal conversion efficiency and exergetic efficiency, respectively relative to the base fluid (distilled water). The enhancement is show to be higher for the exergetic efficiency than it is for the photothermal conversion efficiency.

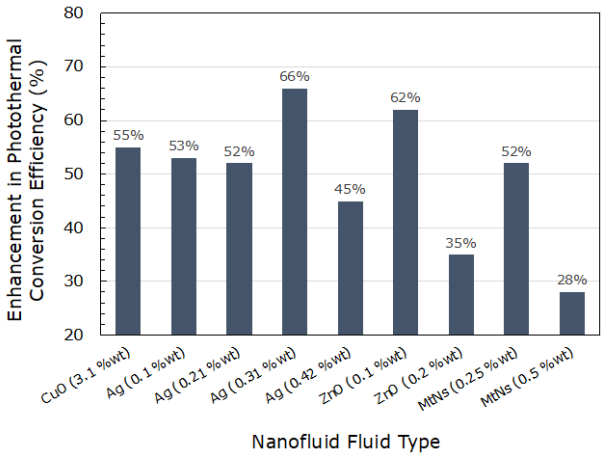

Fig. 11: Enhancement in photothermal average conversion efficiency.

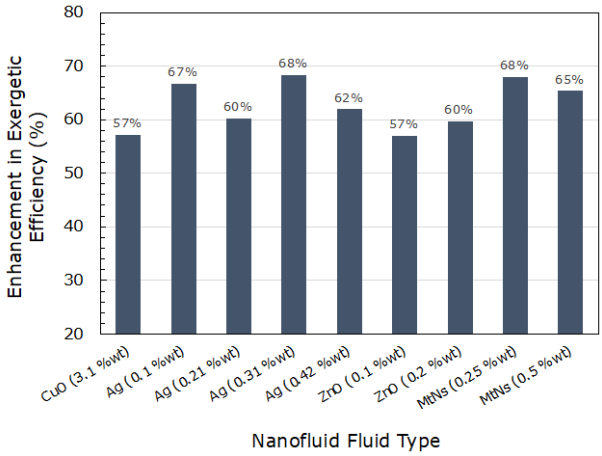

Fig. 12: Enhancement in the average exergetic efficiency.

5. Conclusion

An experimental study was performed to evaluate the thermal and exergetic efficiencies of CuO, Ag, ZnO, and MtNs nanofluids at different nanoparticle concentrations with the use of a solar simulator. The nanofluids were subjected to an average heat flux of 800 W/m^2. The enhancement in the nanofluid thermal and exergetic efficiency was compared to that of the base fluid, distilled water. Based on the results of the study, the following conclusions were reached:

- The photothermal conversion efficiency was shown to peak at relatively low nanoparticle concentrations (0.31% wt for Ag, 0.1% wt for ZnO, and 0.25% wt for MtNs). The photothermal conversion efficiency is shown to decrease with the increase in the nanofluid temperature.
- The exergetic efficiency was shown to increase with temperature, reaching a peak near 40 ºC for all nanofluids, and declining afterwards.
- For the same nanoparticle concentration, the enhancement in the average exergetic efficiency of the tested samples was shown to be higher than that of the photothermal conversion efficiency. Both photothermal conversion and exergetic efficiencies were sensitive to the nanoparticle concentration.
- Among the best performing nanofluids, silver had the highest thermal and exergetic efficiency (an average of 66% and 68%, respectively) that was attained at a concentration of 0.31% by weight.

References

[1] M. Gao, L. Zhu, C.K.N. Peh, and G.W. Ho, "Solar absorber material and system design for photothermal water vaporization towards clean water and energy production," *Energy Environ. Sci.*, vol. 12, pp. 841-864, 2019.

[2] T. Boldoo, J. Ham, E. Kim, and H. Cho, "Review of the photothermal energy conversion performance of nanofluids, their applications, and recent advances," *Energies*, vol. 13, pp. 1-33, 2020.

[3] Z. Luo, C. Wang, W. Wei, G. Xiao, and M. Ni, "Performance improvement of a nanofluid solar collector based on direct absorption collection (DAC) concepts," *Int. J. Heat Mass Transf.*, vol. 75, pp. 262-271, 2014.

[4] M. Amjad, H. Jin, X. Du, and D. Wen, "Experimental photothermal performance of nanofluids under concentrated solar flux," *Sol. Energy Mater. Sol. Cells*, vol. 182, pp. 255-262, 2018.

[5] T. Yousefi, F. Veysi, E. Shojaeizadeh, and S. Zinadini, "An experimental investigation on the effect of Al_2O_3-H_2O nanofluid on the efficiency of flat-plate solar collectors," *Renew. Energy*, vol. 39, pp. 293-298, 2012.

[6] H. Zhang, H-J. Chen, X. Du, and D. Wen, "Photothermal conversion characteristics of gold nanoparticle dispersions," *Sol. Energy*, vol. 100, pp. 141-147, 2014.

[7] T. Wang, G. Tang, and M. Du, "Photothermal conversion enhancement of triangular nanosheets for solar energy harvest," *Appl. Therm. Eng.*, vol. 173, 2020.
[8] M. Chen, Y. He, J. Huang, and J. Zhu, "Investigation into Au nanofluids for solar photothermal conversion," *Int. J. Heat Mass Transf.*, vol. 108, pp. 1894-1900, 2017.
[9] H. Jin, G. Lin, L. Bai, M. Amjad, E. Filho, and D. Wen, "Photothermal conversion efficiency of nanofluids: An experimental and numerical study," *Sol. Energy*, vol. 139, pp. 278-289, 2016.
[10] M. Amjad, G. Raza, Y. Xin, S. Pervaiz, J. Xu, X. Du, and D. Wen "Volumetric solar heating and steam generation via gold nanofluids," *Appl. Energy*, vol. 206, pp. 393-400, 2017.
[11] X. Wang, Y. He, X. Liu, L. Shi, and J. Zhu, "Investigation of photothermal heating enabled by plasmonic nanofluids for direct solar steam generation," *Sol. Energy*, vol. 157, pp. 35-46, 2017.
[12] M. Moravej, M. Doranehgard, A. Razeghizadeh, F. Namdarnia, N. Karimi, L. Li, H. Mozafari, and Z. Ebrahimi, "Experimental study of a hemispherical three-dimensional solar collector operating with silver-water nanofluid," *Sustain. Energy Technol. Assess.*, vol. 44, 2021.
[13] M. Chen, Y. He, J. Zhu, and D. Wen, "Investigating the collector efficiency of silver nanofluids based direct absorption solar collectors," *Appl. Energy*, vol. 181, pp. 65-74, 2016.
[14] M. Chen, Y. He, J. Zhu, Y. Shuai, B. Jiang, and Y. Huang, "An experimental investigation on sunlight absorption characteristics of silver nanofluids," *Sol. Energy*, vol. 115, pp. 85-94, 2015.
[15] J. Wen, X. Li, W. Chen, and J. Liu, "Systematical investigation on the solar-thermal conversion performance of TiN plasmonic nanofluids for the direct absorption solar collectors," *Colloids Surf. A: Physicochem. Eng. Asp.*, vol. 624, 2021.
[16] J. Zeng, and Y. Xuan, "Enhanced solar thermal conversion and thermal conduction of MWCNT-SiO_2/Ag binary nanofluids," *Appl. Energy*, vol. 212, pp. 809-819, 2018.
[17] J. Gao, W. Yu, H. Xie, and O. Mahian, "Graphene-based deep eutectic solvent nanofluids with high photothermal conversion and high-grade energy," *Renew. Energy*, vol. 190, pp. 935-944, 2022.
[18] J. Ham, Y. Shin, and H. Cho, "Comparison of thermal performance between a surface and a volumetric absorption solar collector using water and Fe_3O_4 nanofluid," *Energy*, vol. 239, 2022.
[19] L. Wang, M. Wang, Z. Xu, W. Yu, and H. Xie, "Well oil dispersed Au/oxygen-deficient TiO_2 nanofluids towards full spectrum solar thermal conversion," *Sol. Energy Mater. Sol. Cells*, vol. 212, 2020.
[20] L. Chen, C. Xu, J. Liu, X. Fang, and Z. Zhang, "Optical absorption property and photothermal conversion performance of graphene oxide/water nanofluids with excellent dispersion stability," *Sol. Energy*, vol. 148, pp. 17-24, 2017.
[21] Z. Li, A. Kan, K. Wang, Y. He, N. Zheng, and W. Yu, "Optical properties and photothermal conversion performances of graphene based nanofluids," *Appl. Therm. Eng.*, vol. 203, 2022.
[22] Z. Hong, J. Pei, Y. Wang, B. Cao, M. Mao, H. Liu, H. Jiang, Q. An, X. Liu, and X. Hu, "Characteristics of the direct absorption solar collectors based on reduced graphene oxide nanofluids in solar steam evaporation," *Energy Convers. Manag.*, vol. 199, 2019.
[23] H. Zhang, K. Wang, L. Wang, H. Xie, and W. Yu, "Mesoporous CuO with full spectrum absorption for photothermal conversion in direct absorption solar collectors," *Sol. Energy*, vol. 201, pp. 628-637, 2020.
[24] www.mars-hydro.com, data retrieved December 1, 2022.
[25] Y. Xuan and W. Roetzel, "Conceptions for heat transfer correlation of nanofluids," Int. J. Heat Mass Trans., vol. 43, no. 19, pp. 3701-3707, 2000.